DOI: 10.1002/((please add manuscript number))
Article type: Communication

Organic diode rectifiers based on high performance conjugated polymer for near-field energy harvesting circuit

*Stuart G. Higgins, Tiziano Agostinelli, Steve Markham, Robert Whiteman and Henning Sirringhaus**

Dr. S. G. Higgins,[+] Prof. H. Sirringhaus
Cavendish Laboratory, University of Cambridge, J. J. Thomson Avenue, Cambridge, CB3 0HE, UK.
Email: hs220@cam.ac.uk

Dr. T. Agostinelli,[*] S. Markham
FlexEnable Ltd, 34 Cambridge Science Park, Milton Road, Cambridge, CB4 0FX, UK.

Dr. R. Whiteman
De La Rue plc, Overton, Basingstoke, RG25 3JG, UK.

[+] Present address: Department of Materials and Department of Bioengineering, Imperial College London, London, SW7 2AZ, UK.

[*] Present address: Endomagnetics Ltd, Jeffreys Building, St John's Innovation Park, Cambridge, CB4 0WS, UK.

Keywords: energy harvesting, organic diodes, organic semiconductors, RFID, NFC

We report organic diodes manufactured on a plastic substrate capable of rectifying a high-frequency radio-frequency identification (HF RFID) signal (13.56 MHz), with sufficient power to operate an interactive smart tag. We combine a high performance conjugated semiconductor (an indacenodithiophene–benzothiadiazole copolymer, C_{16}IDT-BT) with a carefully optimized architecture to satisfy the electrical requirements for an organic semiconductor-based logic chip.

Organic semiconductors have been used extensively in organic field-effect transistors (OFETs),[1] organic photovoltaics (OPVs),[2] and organic light-emitting diodes (OLEDs).[3] The use of organic semiconductors in rectifiers is less frequently reported, despite being one of the key components in energy harvesting circuits. Rectifiers convert an alternating current (AC) into a direct current (DC). They are found in many electrical systems, including RFID tags. An antenna on the tag couples to a near-field communication (NFC) field generated by a transmitter, and the rectifying circuit converts this oscillating signal into a DC bias that can be used to wirelessly power the tag's internal circuitry.[4] Organic rectifiers are an important application of organic electronics.[5–9] Not only do organic rectifiers share the general benefits of organic electronics (high throughput manufacturing and flexibility) but they also have the potential to undercut the cost of attaching silicon chips to printed antennas, which currently places an upper bound on the manufacturing price of silicon-based RFID tags.[4] However, despite advances in OFET and OLED powered flexible displays,[10] lighting,[11] and photovoltaics,[2] organic rectifiers have so far failed to be adopted in the same way.

One of the most highly cited works on organic diodes is that of Steudel *et al.*,[5] where they demonstrate evaporated pentacene diodes operating at 50 MHz. The authors subsequently went on to highlight the intrinsic benefits of using organic diodes, rather than OFETs, for rectification.[12] Since that point, numerous variants have been presented. Heljo *et al*.

demonstrated printed half- and full-wave rectifiers from poly(triarylamine) (PTAA), with copper and silver electrodes.[13] While diodes have also been demonstrated with significantly higher operational speeds, including coplanar nanodiodes well in excess of 20 MHz,[14] evaporated C_{60} diodes,[15] and evaporated pentacene diodes at 1 GHz,[7] the relatively low operating voltages and power of these devices under load (< 5 V) becomes an issue when trying to combine these approaches with organic semiconductor-based logic.

Our aim in this work is to develop a rectifier that can power a unipolar logic circuit, based on p-type organic field-effect transistors, from the NFC field that is available from a mobile phone. In addition, the circuit features a four-segment electrochromic display, which must also be powered by the rectifier. SPICE simulations of this circuit show that, as well as operating at 13.56 MHz, the diodes need to yield a current density of J_{on} >1 A cm^{-2} at +5 V, with a diode capacitance of $C_D \leq 5$ pF. As well as sustaining the forward current density, the diodes also need to survive a reverse bias of $V \leq -15$ V, to achieve the required voltage output of $V_{out} \approx +15$ V for the organic logic. These are very stringent requirements, which are not met by some of the nominally very high frequency printed diodes demonstrated in the literature. As a result, some researchers have moved away from organic semiconductors, towards inorganic,[16] and metal-oxide based rectifiers.[17,18] While metal oxides are useful in many contexts, the additional complexity associated with processing a non-organic material and the temperatures involved may not be compatible with low-cost manufacture on flexible substrates. Here we demonstrate how by using an intrinsically high mobility, solution-processable conjugated polymer semiconductor we can realize high-performance diodes with materials that are fully compatible with organic thin-film transistor (OTFT) manufacturing and meet all the requirements for NFC applications.

Our diode architecture and typical current-voltage characteristics are shown in **Figure 1.** We use an indacenodithiophene-benzothiadiazole copolymer (C_{16}IDT-BT) with a simple gold metal as a bottom cathode and a MoO_3/Ag top electrode as anode, on a planarized polyethylene naphthalate (PEN) substrate.[19,20] The rigid polymer backbone of C_{16}IDT-BT minimizes energetic disorder, facilitating intra-chain charge transport, and resulting in high intrinsic mobilities.[21] In this way, C_{16}IDT-BT is well suited to solution-processed organic electronics, where amorphous films can provide the necessary performance. While well-used for OFETs, C_{16}IDT-BT remains under-explored as a material system for organic diodes. In this simple architecture, we achieve a high forward current density of 6 A cm^{-2} at relatively low forward voltages of +5 V. The diodes also exhibit a high rectification ratio > 10^6 between −5 V and +5 V. More importantly the rectification ratio between −15 V and +5 V, which is most relevant in our application, is > 10^2 and the diodes exhibit a high reverse breakdown voltage ($V_{\mathrm{break}}^{\mathrm{rev}}$< −15 V) (**Figure 1b**). In these measurements, the gold cathode is held at ground, while the voltage applied to the silver anode is swept from negative to positive.

It may seem peculiar that we use such a simple diode architecture, in particular the choice of an unmodified gold electrode as a cathode. The use of gold is convenient as it is commonly used as an electrode material in OTFT circuits. However, typical diode optimization strategies include introducing hole and electron transport layers at the anode and cathode interfaces respectively to aid charge injection and/or improve rectifying behavior. Zinc oxide (ZnO) is a common electron-transporting material used in this respect and as an n-type semiconductor.[6,22] We initially fabricated devices with zinc oxide (ZnO) deposited via atomic layer deposition (ALD) onto the gold cathode, where monolayers of ZnO were sequentially grown on top of the gold electrode.[22] However, during testing we observed that while ZnO, was effective at reducing the off-current by approximately four orders of magnitude (and thus increasing the reverse breakdown voltage), it did so at the expense of on-

current (see **Figure 2a**), rendering the diodes ineffective for our application. Growing ALD layers on top of a plastic substrate also introduced additional complexity and process variation which is undesirable in a manufacturing environment.

Similarly, polyethylenimine ethoxylated (PEIE) was explored as a potential interlayer. PEIE is a polymer that has been shown to induce a large dipole moment at the interface of multiple materials, including gold, aiding electron injection.[23] However, despite a reduction in off-current a similar reduction in on-current was seen again (see Figure 2b). Note that in Figures 2a and 2b, it appears that for some devices the current minimum (as indicated by the inflexion point in the logarithmic plot) is < 0 V. However, these transitions are occurring for extremely small current values ~<10 pA, which are approaching the noise floor of our DC measurement setup. Therefore, we attribute this as an artefact of stray capacitance and charging effects in the measurement, rather than meaningful device behavior.

In addition to the reduction in on-current, devices with PEIE layers were found to be unstable under test. It was also initially envisaged that replacing the gold cathode with silver might further improve diode rectification ratios. Silver has a lower work function than gold and therefore theoretically should act as a greater barrier to hole injection at the cathode, reducing off-current. However, we found that while there was no significant change in diode on-current, the off-current increased slightly (see **Supporting Figure S1**). We additionally saw greater variation in the device characteristics. We attribute this to the susceptibility of the silver cathode to oxidize during the fabrication process.

After optimizing the process in this way, we concluded that the very simple and somewhat unconventional device architecture provided the best performance that allowed us to meet simultaneously the application requirements of high on-current, rectification ratio and

breakdown voltage. The top silver electrode with a molybdenum trioxide (MoO_3) interlayer acts as an anode and provides an Ohmic contact to the polymer while the bare gold bottom electrode without any interfacial modification act as a cathode and provides the small Schottky barrier necessary to achieve rectification. The rectification is provided by the relative difference in hole injection from the MoO_3/Ag electrode under forward bias and the hole injection from Au under reverse bias. An approximate energy level diagram for our device architecture is shown in **Supporting Figure S2.**[19,24,25] This simple approach is beneficial from a manufacturing perspective, as gold and silver are environmentally sufficiently stable and can be easily integrated into designs on plastic substrates that provide only limited encapsulation and also incorporate OFETs and other components that are normally processed in ambient air.

Another benefit of using gold and silver electrodes with similar work functions is a reduction in built-in voltage across the diode, which is formed by the relative difference between anode and cathode work functions. This minimizes the built-in voltage, resulting in fast-turn of the diodes. We see very low transition voltages $V_T < 0.1$ V. This is important because low voltage drops across the diode maximizes the output voltage that can be achieved in a rectifying circuit.[7,15]

Figure 3a shows the capacitance-voltage characteristics of the diodes, showing a constant capacitance in the reverse bias regime of $C_D = 2.5$ pF. One strategy to increase the on-current in a diode is to increase the diode area. However, this simultaneously increases the capacitance of the diode, limiting the maximum operating frequency before capacitive losses render the rectifier ineffective. SPICE simulations of the rectifier indicated the optimum diode area for our devices to be $A \approx 0.02$ mm^2. Fundamentally the diode capacitance (C_D) should be much less than the load capacitance (C_L), which is the equivalent capacitance that the circuit

connected to the rectifier can be considered as, to facilitate a stable voltage output (i.e. $C_D << C_L$).[5] For our circuit this is dominated by a smoothing capacitor, used to regulate the current drawn by the circuit, hence $C_L \approx 1$ nF, satisfying this requirement.

Figure 3a also shows that the measured capacitance rises from 2-3 pF in reverse bias to 6-7 pF as the diode is forward biased. Kim *et al.* have previously observed a small increase in capacitance (~0.3 pF) in forward-biased pentacene diodes, which they attributed to trapped charge inside the semiconductor in this regime.[26] We see a larger increase in our devices, with the capacitance rising by ~3 pF. This may be due to a contribution from trapped charge, however it's also likely that the increasing current distorts the impedance measurement used to determine the capacitance. As the diode enters the forward regime, the phase angle of the impedance drops from ~90º (capacitive behavior) to ~0º (conductive behavior), as shown in **Supporting Figure S3**. With increasing conductivity, the diode impedance drops below ~10 kΩ and the measurement falls outside our equipment specification for the parallel *RC* circuit model. Hence the value of the capacitance in this region cannot be considered meaningful.[27]

We tested the frequency response of single diodes in a half-wave rectifier configuration, with the measured voltage output shown in **Figure 3b**. Diodes were connected in parallel with a smoothing capacitor and load resistor and stimulated with a sinusoidal input (V_{in} = 20 V_{p-p}). Our diodes show a slight increase in output with increasing frequency, up to ~3 MHz, above which there is a slight roll-off. The origin of the increase in output voltage with frequency is not clear at present, it may possibly be due to the injected charges carriers no longer being able to equilibrate with shallow traps in the polymer at higher frequencies. For a low impedance load, R_{load} = 100 kΩ, V_{out} = +2.9 V at 13.56 MHz, increasing to V_{out} = +5.1 V for R_{load} = 10 MΩ. Four diodes were connected in a quadrupler configuration, as illustrated in

Figure 3c. From this the voltage output of the quadrupler into a high impedance load was measured, with a maximum of V_{out} = +16.1 V for an input of V_{in} = 20 $V_{p\text{-}p}$.

Although these diodes were fabricated explicitly to comply with the HF RFID standard and we have not had access to a test setup that is able to measure performance at higher frequencies beyond 13.56 MHz, it is nonetheless interesting to consider their upper frequency limit. Estimating the frequency response of organic diodes is challenging due to the complexity and non-ideal nature of their behavior.[28] A common approach is to consider the inverse of the carrier transit time across the diode layer to estimate a cutoff frequency (f_C):

$$f_C = \frac{\mu(V_A - V_{out})}{L^2} \quad (1)$$

where L is the semiconductor thickness, μ is the mobility, and V_A is the peak voltage applied to the diode.[5,28] With a conservative, lower bound estimate of the vertical mobility of C_{16}IDT-BT of μ = 0.001 $cm^2\ V^{-1}\ s^{-1}$ (see discussion below) equation (1) gives an estimate of f_C > 125 MHz (where V_A = +20 V, V_{out} = +6 V, L = 106 nm). An alternative estimate can be derived by considering the current flowing through the device during the forward sweep of the input source, as derived by Steudel *et al.*:

$$f_C = \frac{9\mu}{16\pi L^2 V_{out}}\left[(-3V_{out} + V_T)\sqrt{V_A^2 - (V_{out} + V_T)^2} + (V_A^2 + 2V_{out}^2)\arccos\left(\frac{V_{out}+V_T}{V_A}\right)\right].^{[5,7]} \quad (2)$$

Equation (2) gives an estimate of f_C > 68 MHz. This is an approximation, as the diode is not operating in the SCLC regime and has a non-zero leakage current, hence the dynamic behavior is expected to be more complex. However, it supports the experimental results below that the cutoff frequency is significantly higher than the required 13.56 MHz.

We noted a small increase in reverse-current and a correspondingly larger increase in forward-current in the IV characteristics of the diodes immediately post-fabrication, even when stored in a nitrogen atmosphere (see **Supporting Figure S4).** Further testing found that this shift could be forced to occur more rapidly by biasing the device, with an increase of ~4 nA s^{-1} in on-current (biased at +5 V) observed (see **Supporting Figure S5**). This behavior appears to stabilize after a few hours. The origin is unclear, but could be due to diffusion of either the MoO_3 into the semiconductor layer, or Ag into the MoO_3 layer. It has previously been observed that MoO3 diffuses into organic semiconductor layers, forming a doping layer at the interface.[24] Similarly, studies on the diffusion of both Au and Ag have shown that vacuum deposited layers can readily diffuse into and form complex interfaces with previously deposited layers.[29,30] It may be that the gradual penetration of either Ag or MoO_3 into the layer results in a shift in the relative injection barrier at this interface. Further optimization of the MoO_3 layer also revealed that the interlayer thickness is critical to device performance. As the layer thickness increases, both diode forward and reverse current decrease (see **Supporting Figure S6**). This suggests that beyond an initial doping effect, any additional MoO_3 acts simply as a series resistance, lowering the current flow through the device.

The long-term stability of the rectifier output was also explored under constant use over a period of hours. Diodes were connected in parallel with a capacitor to form a smoothed half-wave rectifier, stimulated with a sinusoidal input (V_{in} = 20 $V_{p\text{-}p}$), and the DC output voltage of this circuit measured. A slow degradation was observed with time, with the output voltage for a single-stage rectifier dropping from V_{out} = +6 V to +5 V after approximately two and half hours, a degradation rate of $\Delta V \approx 0.4$ V per hour continuous use (see **Supporting Figure S7**). This level of degradation is acceptable for our application, and could potentially be further improved through the use of molecular additives, which have recently been shown to stabilize

C_{16}IDT-BT films in OFETs.[31] It was noted that the output voltage recovered slightly after the bias was removed and reapplied later, suggesting at least some of this degradation is reversible.

Forward breakdown in the organic diodes was typically observed when DC voltages of $V \approx$ +6 V were applied, which we attribute to Joule heating. This is observed in optical micrographs of the devices after breakdown, which show clear signs of thermal effects (see **Supporting Figure S8**). This is in part a limitation of using plastic substrates, which have low thermal conductivities and don't conduct heat away as rapidly as substrates such as silicon. Interestingly however, we found that although the forward breakdown voltage of our diodes is lower than the peak input voltage ($V_{\text{break}}^{\text{fwd}} < |V_{\text{in}}|$), as determined from quasi-static DC measurements, the diodes were more than sufficient for use in a rectifier operating with V_{in} = 20 $V_{p\text{-}p}$. We attribute this in part to the lower average power transferred by an AC signal, but mainly to the behavior of the rectifier under load. The lower impedance of the diode in the forward regime results in less voltage drop across the device, compared to the reverse regime. Hence it's possible to operate a diode with $V_{\text{break}}^{\text{fwd}} < |V_{\text{in}}|$ effectively without issue, but still requiring $V_{\text{break}}^{\text{rev}} > |V_{\text{in}}|$ in order to sustain the full reverse sweep voltage.

The voltage breakdown requirements had important implications for the design and optimization of the diodes presented here. Rather than optimizing for a symmetric rectification ratio, the more important figure of merit was the ratio between the measured absolute current density at –15 V, and +5 V. In our application, simulations suggested this ratio must exceed 10 for the diode to operate properly as a rectifier.

To demonstrate the effectiveness of our approach, we fabricated a voltage quadrupler to power an interactive smart tag. Our application example is an authentication label; the user powers-up the tag using an NFC source, for example a smartphone or NFC reader (Figure 3e). The tag comprises resistive touch input buttons, OFET-based logic, and electrophoretic output displays (Figure 3f). An alternating current is induced in an antenna, when the tag is placed in a 13.56 MHz RF field. A user then inputs a two-digit code using the in-built keypad. The logic circuit checks if this code is the same as a pre-programmed reference, and returns a pass/fail indicator accordingly (see **Supporting Movie S1** for a video demonstrating the smart tag in action). In Figure 3f and Supporting Movie S1 the tag is powered wirelessly using an USB-powered industry-standard NFC reader, demonstrating the validity of our approach.

Each stage of the voltage quadrupler rectifies the signal, and sequentially increases the voltage, so the DC output is approximately four times that of each constituent diode. The voltage quadrupler can power the logic circuit, which has an equivalent load of $R_{load} \approx$ 320 kΩ, at V = +16 V, thus validating the overall approach to the diode optimization.

Although we clearly achieve the target rectification and application for our organic diodes, there is still scope for further optimization. While we can reach high on-currents at low voltages, the diodes we have fabricated do not obey the square-law relationship for space-charge limited current (SCLC) density, J, as shown in equation (3):

$$J = \frac{9}{8}\mu\varepsilon_0\varepsilon_r\frac{V^2}{L^3} \quad (3)$$

where ε_0 is the permittivity of free space, ε_r is the relative permittivity of the semiconductor, and V is the voltage across the diode.[32] The devices shown in Figure 1 don't agree well with equation 3 (see **Supporting Figure S9**), suggesting that the diodes are not yet operating in a SCLC regime. This may in part be due to a voltage dependent mobility, or the presence of

charge traps within the semiconductor, such that the device is still operating in a trap-filling regime.[33] Attempts to measure the devices at higher voltages failed because devices breakdown under the very high current density before the SCLC regime is reached. Extracting a precise value for the intrinsic mobility is not straightforward from our data, however by modelling equation (1) for a diode with equivalent parameters and assuming the SCLC regime gives the theoretical limit of current density, we estimate the lower bound for the SCLC mobility, $\mu_{SCLC} > 0.001$ cm^2 V^{-1} s^{-1} (see Supporting Figure S9). Given that this is three orders of magnitude lower than the field-effect mobility obtained in C_{16}IDT-BT OFETs (μ_{FET} = 1.5 – 2.5 cm^2 V^{-1} s^{-1}) it suggests that reducing traps, again potentially through the use of molecular additives, could yet further enhance the performance of the diodes.[21,31]

We have demonstrated high performance conjugated polymer rectifying diodes on a plastic substrate that is suitable for NFC applications. Optimizing for high diode forward-currents, even at the expense of increased reverse-current, was found critical for reaching the necessary diode performance and necessitated the use of a very simple diode architecture based on a gold cathode and MoO_3/silver anode. We have exploited these diodes in both half-wave rectifiers with an output of V_{out} = +6 V, for a V_{in} = 20 $V_{p\text{-}p}$, and in a voltage quadrupler circuit operating at 13.56 MHz. The combined energy harvesting circuit was sufficient to power an organic-semiconductor based logic circuit, to enable an interactive smart tag powered by a standard NFC card reader.

Experimental Section

Fabrication of Organic Diodes: Organic diodes were fabricated on a planarized polymer PEN substrate. The surface roughness of this substrate was found to be critical; for R_q > 10 nm RMS, device yield dropped substantially due to shorts occurring between the cathode and anode. The substrate was sonicated in 2-propanol for 10 minutes and then dried with nitrogen

gas. The substrate was baked at 90°C for 10 minutes, to minimize the impact from potential degassing of water vapor from the substrate. A 5 nm thick adhesion layer of chromium (chrome plated tungsten rod, Testbourne Ltd) followed by a 50 nm thick gold layer (99.99% purity evaporated from a tungsten boat, Testbourne Ltd) were thermally evaporated consecutively through a shadow mask onto the substrate to form the cathode. A 15 mg mL^{-1} solution of C_{16}IDT-BT (supplied by the group of Prof. Iain McCulloch at Imperial College London) in 1,2-dichlorobenzene and chloroform (75:25 v/v) was prepared. While C_{16}IDT-BT is readily soluble in many organic solvents, to ensure complete dissolution the solution was heated on a hotplate at 70°C for approximately one hour. The solution was filtered through a 0.45 µm polytetrafluoroethylene filter immediately before spin-coating. Substrates were mounted on a glass carrier and spin-coated with the heated solution, using a ramped program with a nominal value of 1400 rpm for 120 s. These parameters gave a semiconductor layer of thickness $L \approx 106$ nm, as determined by surface profilometry (Dektak 3, Veeco). Excess semiconductor was removed from the cathode contact pads using swabs soaked in anhydrous toluene. A 2 nm thick layer of MoO_3 (2-4 mm pieces, 99.95% purity, Testbourne Ltd), followed by a 50 nm thick layer of Ag (1-3 mm pellets, 99.99% purity, Testbourne Ltd) were thermally evaporated consecutively through a shadow mask to form the anode. All steps from solution preparation onwards were carried out within nitrogen gloveboxes to control for environmental effects. The cathode and anode have nominal widths of 100 µm and 200 µm respectively, resulting in a device area of $A \approx 0.02$ mm^2.

Electrical testing: The quasi-static IV characteristics of the diodes were measured using a semiconductor parameter analyzer (step size $\Delta V = 0.1$ V, Agilent 4155B). The capacitance-voltage characteristics were measured using an impedance analyzer (HP 4192A) at a frequency of $f = 50$ kHz with an oscillator amplitude of 1 V, with the capacitance calculated directly by the impedance analyser using a parallel equivalent circuit. The output voltage of

the diodes were measured as a half-wave rectifier, by placing in series with a capacitor (C_L = 1 nF) and resistor (varied in the range R_L = 100 kΩ - 10 MΩ), using a digital multimeter (Fluke 87V) and an oscilloscope to monitor the ripple voltage.

Smart tag testing: Diodes were encapsulated using an adhesive barrier layer placed over the device region. Diodes were either connected via a zero-insertion force (ZIF) connector or bonded to a motherboard for testing. The smart tag was placed on top of an NFC card reader (SCM Microsystems) for testing.

Supporting Information

Supporting Information is available from the Wiley Online Library or from the authors.

Acknowledgements

S.G.H. acknowledges the support and scientific discussions of M. Nikolka, D. Harkin, G. Schweicher and V. Pecunia, and the extensive technical support of R. Chakalov, R. Beadle and R. Gymer. This work was funded by Innovate UK as part of the project “Security tags Enabled by near field Communications United with Robust Electronics” (SECURE), project number 102026.

Received: ((will be filled in by the editorial staff))
Revised: ((will be filled in by the editorial staff))
Published online: ((will be filled in by the editorial staff))

References

[1] H. Sirringhaus, *Adv. Mater.* **2014**, *26*, 1319.

[2] K. Leo, *Nat. Rev. Mater.* **2016**, *1*, 16056.

[3] W. Brütting, J. Frischeisen, T. D. Schmidt, B. J. Scholz, C. Mayr, *Phys. Status Solidi Appl. Mater. Sci.* **2013**, *210*, 44.

[4] V. Subramanian, in *Inkjet Technol. Digit. Fabr.* (Eds.: I.M. Hutchings, G.D. Martin), John Wiley & Sons Ltd, Chichester, **2013**, pp. 255–274.

[5] S. Steudel, K. Myny, V. Arkhipov, C. Deibel, S. De Vusser, J. Genoe, P. Heremans, *Nat. Mater.* **2005**, *4*, 597.

[6] B. N. Pal, J. Sun, B. J. Jung, E. Choi, A. G. Andreou, H. E. Katz, *Adv. Mater.* **2008**, *20*, 1023.

[7] C. Kang, J. Wade, S. Yun, J. Lim, H. Cho, J. Roh, H. Lee, S. Nam, D. D. C. Bradley, J.-S. Kim, C. Lee, *Adv. Electron. Mater.* **2016**, *2*, 1500282.

[8] C. Y. Lin, C. H. Tsai, H. T. Lin, L. C. Chang, Y. H. Yeh, Z. Pei, Y. R. Peng, C. C. Wu, *Org. Electron.* **2011**, *12*, 1777.

[9] P. Heljo, K. E. Lilja, H. S. Majumdar, D. Lupo, *Org. Electron.* **2014**, *15*, 306.

[10] G. Gelinck, P. Heremans, K. Nomoto, T. D. Anthopoulos, *Adv. Mater.* **2010**, *22*, 3778.

[11] H. Sasabe, J. Kido, *J. Mater. Chem. C* **2013**, *1*, 1699.

[12] S. Steudel, S. De Vusser, K. Myny, M. Lenes, J. Genoe, P. Heremans, *J. Appl. Phys.* **2006**, *99*, DOI 10.1063/1.2202243.

[13] P. S. Heljo, M. Li, K. E. Lilja, H. S. Majumdar, D. Lupo, *IEEE Trans. Electron Devices* **2013**, *60*, 870.

[14] J. Semple, S. Rossbauer, C. H. Burgess, K. Zhao, L. K. Jagadamma, A. Amassian, M. A. McLachlan, T. D. Anthopoulos, *Small* **2016**, *12*, 1993.

[15] D. Im, H. Moon, M. Shin, J. Kim, S. Yoo, *Adv. Mater.* **2011**, *23*, 644.

[16] N. Sani, M. Robertsson, P. Cooper, X. Wang, M. Svensson, P. Andersson Ersman, P.

Norberg, M. Nilsson, D. Nilsson, X. Liu, H. Hesselbom, L. Akesso, M. Fahlman, X. Crispin, I. Engquist, M. Berggren, G. Gustafsson, *Proc. Natl. Acad. Sci. U. S. A.* **2014**, *111*, 85.

[17] J. Zhang, Y. Li, B. Zhang, H. Wang, Q. Xin, A. Song, *Nat. Commun.* **2015**, *6*, 7561.

[18] K. Myny, B. Cobb, J.-L. van der Steen, A. K. Tripathi, J. Genoe, G. Gelinck, P. Heremans, in *2015 IEEE Int. Solid-State Circuits Conf. - Dig. Tech. Pap.* (Eds.: J. Anderson, D. Dunwell, V. Gaudet, G. Gulak, J. Haslett, K. Pagiamtzis, K.C. Smith), IEEE, San Francisco, CA, **2015**, pp. 1–3.

[19] W. Zhang, J. Smith, S. E. Watkins, R. Gysel, M. McGehee, A. Salleo, J. Kirkpatrick, S. Ashraf, T. Anthopoulos, M. Heeney, I. McCulloch, *J. Am. Chem. Soc.* **2010**, *132*, 11437.

[20] W. Zhang, Y. Han, X. Zhu, Z. Fei, Y. Feng, N. D. Treat, H. Faber, N. Stingelin, I. McCulloch, T. D. Anthopoulos, M. Heeney, *Adv. Mater.* **2016**, *28*, 3922.

[21] D. Venkateshvaran, M. Nikolka, A. Sadhanala, V. Lemaur, M. Zelazny, M. Kepa, M. Hurhangee, A. J. Kronemeijer, V. Pecunia, I. Nasrallah, I. Romanov, K. Broch, I. Mcculloch, D. Emin, Y. Olivier, J. Cornil, D. Beljonne, H. Sirringhaus, *Nature* **2014**, *515*, 384.

[22] T. Tynell, M. Karppinen, *Semicond. Sci. Technol.* **2014**, *29*, 43001.

[23] S. Höfle, A. Schienle, M. Bruns, U. Lemmer, A. Colsmann, *Adv. Mater.* **2014**, *26*, 2750.

[24] M. C. Gwinner, R. Di Pietro, Y. Vaynzof, K. J. Greenberg, P. K. H. Ho, R. H. Friend, H. Sirringhaus, *Adv. Funct. Mater.* **2011**, *21*, 1432.

[25] B. De Boer, A. Hadipour, M. M. Mandoc, T. Van Woudenbergh, P. W. M. Blom, *Adv. Mater.* **2005**, *17*, 621.

[26] C. H. Kim, O. Yaghmazadeh, D. Tondelier, Y. Bin Jeong, Y. Bonnassieux, G. Horowitz, *J. Appl. Phys.* **2011**, *109*, DOI 10.1063/1.3574661.

[27] Hewlett Packard, *Operation and Service Manual: Model 4192A LF Impedance Analyzer*, Hewlett Packard, Tokyo, **1983**.

[28] S. Altazin, R. Clerc, R. Gwoziecki, J.-M. Verilhac, D. Boudinet, G. Pananakakis, G. Ghibaudo, I. Chartier, R. Coppard, *J. Appl. Phys.* **2014**, *115*, 64509.

[29] S. Fladischer, A. Neuhold, E. Kraker, T. Haber, B. Lamprecht, I. Salzmann, R. Resel, W. Grogger, *ACS Appl. Mater. Interfaces* **2012**, *4*, 5608.

[30] G. Zhang, S. A. Hawks, C. Ngo, L. T. Schelhas, D. T. Scholes, H. Kang, J. C. Aguirre, S. H. Tolbert, B. J. Schwartz, *ACS Appl. Mater. Interfaces* **2015**, *7*, 25247.

[31] M. Nikolka, I. Nasrallah, B. Rose, M. K. Ravva, K. Broch, A. Sadhanala, D. Harkin, J. Charmet, M. Hurhangee, A. Brown, S. Illig, P. Too, J. Jongman, I. McCulloch, J.-L. Bredas, H. Sirringhaus, *Nat. Mater.* **2016**, *16*, 356.

[32] S. M. Sze, K. K. Ng, *Physics of Semiconductor Devices*, John Wiley & Sons, Inc., Hoboken, NJ, USA, **2006**.

[33] J. C. Blakesley, F. a. Castro, W. Kylberg, G. F. A. Dibb, C. Arantes, R. Valaski, M. Cremona, J. S. Kim, J.-S. Kim, *Org. Electron.* **2014**, *15*, 1263.

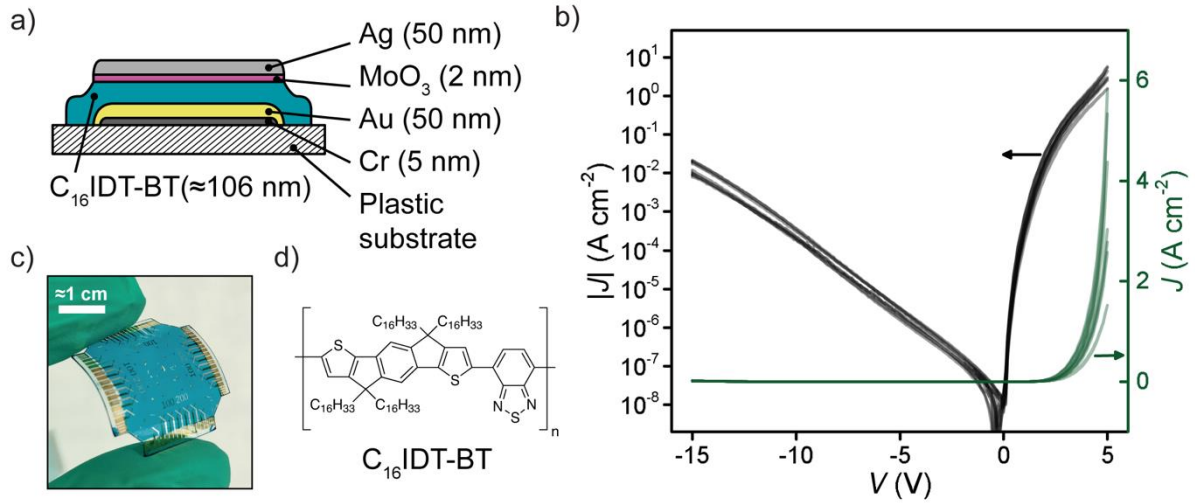

Figure 1. a) Illustration of the diode architecture used with approximate layer thicknesses; b) IV characteristics of organic diodes from the same substrate (plotted on both log/lin and lin/lin scales, 7/7 devices); c) photograph showing an example of a flexible substrate with multiple organic diodes; d) chemical structure of the organic semiconductor used, C_{16}IDT-BT.

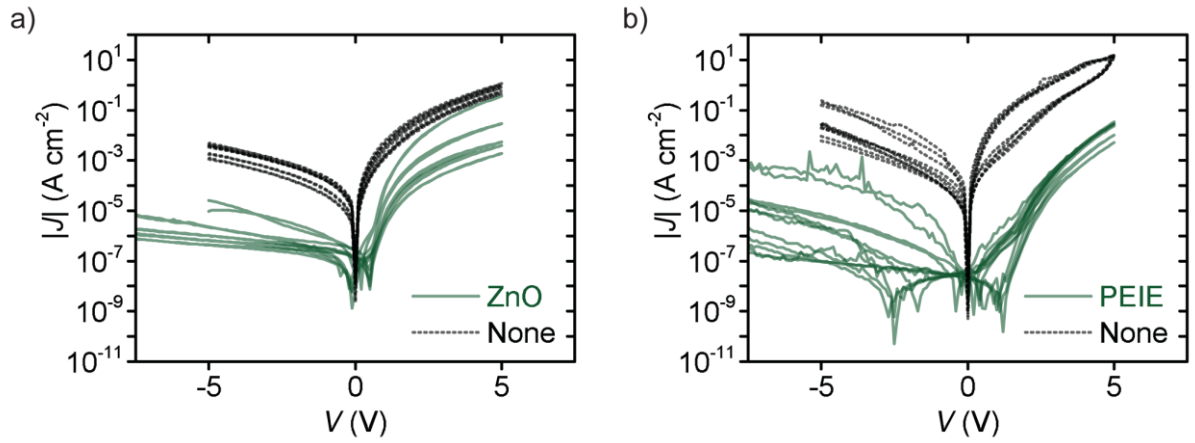

Figure 2. a) IV characteristics of organic diodes fabricated with and without a ZnO interlayer between the cathode and semiconductor (5/6 devices); b) IV characteristics of organic diodes fabricated with and without a PEIE interlayer between the cathode and semiconductor (5/6 devices).

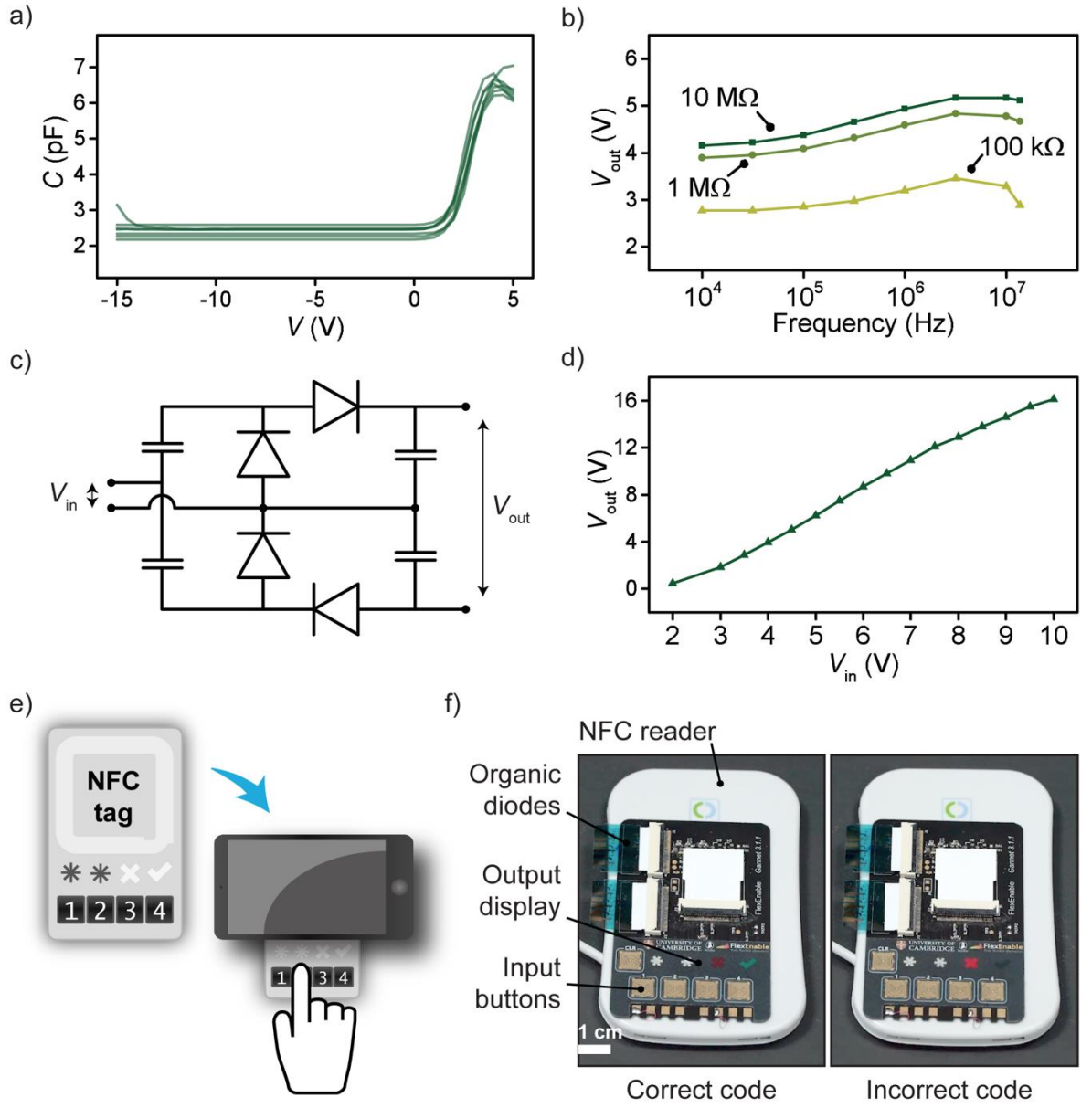

Figure 3. a) Capacitance-voltage characteristics of organic diodes (7/7 devices); b) output voltage obtained from a single diode connected in a half-wave rectifier configuration for differing loads with C_L = 1 nF; c) illustration of the voltage quadrupler used in the final rectifying circuit; d) quadrupler output voltage as a function of sinusoidal input voltage (peak-peak) for a load R_L = 10 MΩ load and stimulus of 50 kHz; e) illustration of the proposed usage scenario of the rectifier in a smart tag; f) photographs of prototype tag placed on top of NFC reader, showing green tick indicator for correct code entry, and red cross indicator for incorrect code entry (organic diode chips shown on left hand side of image).

A high performance conjugated polymer is shown to create fast organic rectifiers, which can be used in a near-field energy-harvesting circuit. The performance of this circuit is sufficient to power an interactive smart-tag from a 13.56 MHz near-field communication source.

energy harvesting, organic diodes, organic semiconductors, RFID, NFC

S. G. Higgins, T. Agostinelli, S. Markham, R. Whiteman, H. Sirringhaus*

Organic diode rectifiers based on high performance conjugated polymer for near-field energy harvesting circuit

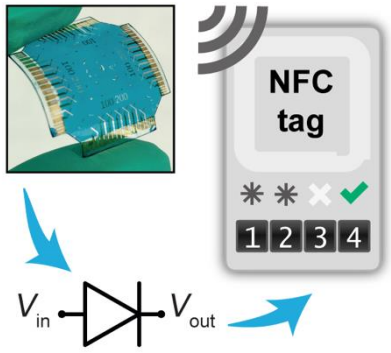

Supporting Information

Organic diode rectifiers based on high performance conjugated polymer for near-field energy harvesting circuit

*Stuart G. Higgins, Tiziano Agostinelli, Steve Markham, Robert Whiteman and Henning Sirringhaus**

Dr. S. G. Higgins,[+] Prof. H. Sirringhaus
Cavendish Laboratory, University of Cambridge, J. J. Thomson Avenue, Cambridge, CB3 0HE, UK.
Email: hs220@cam.ac.uk

Dr. T. Agostinelli,[*] S. Markham
FlexEnable Ltd, 34 Cambridge Science Park, Milton Road, Cambridge, CB4 0FX, UK.

Dr. R. Whiteman
De La Rue plc, Overton, Basingstoke, RG25 3JG, UK.

[+] Present address: Department of Materials and Department of Bioengineering, Imperial College London, London, SW7 2AZ, UK.

[*] Present address: Endomagnetics Ltd, Jeffreys Building, St John's Innovation Park, Cambridge, CB4 0WS, UK.

Supporting Figure S1

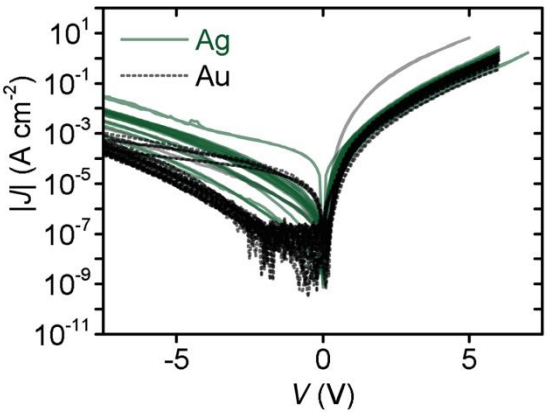

Figure S1. IV characteristics of organic diodes fabricated with either a gold (18/18 devices working) or silver (15/18 devices working) cathode. The silver cathode, while nominally having a more favorable work function was more susceptible to tarnishing during device fabrication, resulting in higher process variability. Note: measurements were made using a shorter integration time for quick characterization, hence the relatively high noise floor at $J \approx 10^{-7}$ A cm^{-2}.

Supporting Figure S2

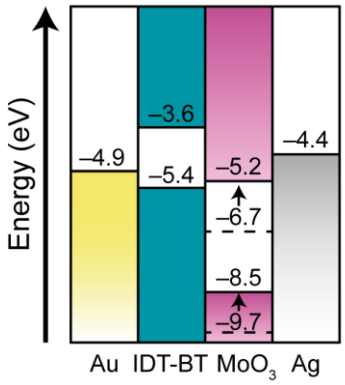

Figure S2. Diagram showing the approximate energy levels for the different materials in the device stack. The HOMO/LUMO levels for C_{16}IDT-BT are estimated from photoelectron spectroscopy and UV-vis measurements of the polymer from the work of Zhang *et al*. The range of values for MoO_3 are from the work of Gwinner *et al.* and represent an approximate range over which the measured energy level can change according to diffusion and clustering of MoO_3 at the interface. The work functions for gold and silver are from the work of de Boer *et al*. For explicit references, see the main text.

Supporting Figure S3

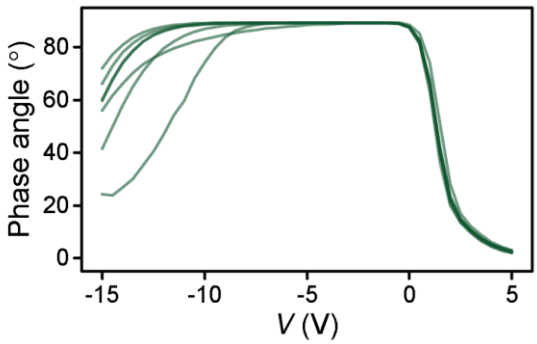

Figure S3. Plot of the measured phase angle for the devices (7/7 devices) shown in Figure 3a. This data shows how the diode behavior is purely capacitive (phase angle ~90º) between –12 V < *V* < 0 V, before transitioning to purely conductive behavior (phase angle ~0º) in the forward bias regime. The gradual decrease in phase angle for *V* < –15 V is a consequence of increasing leakage current in this regime.

Supporting Figure S4

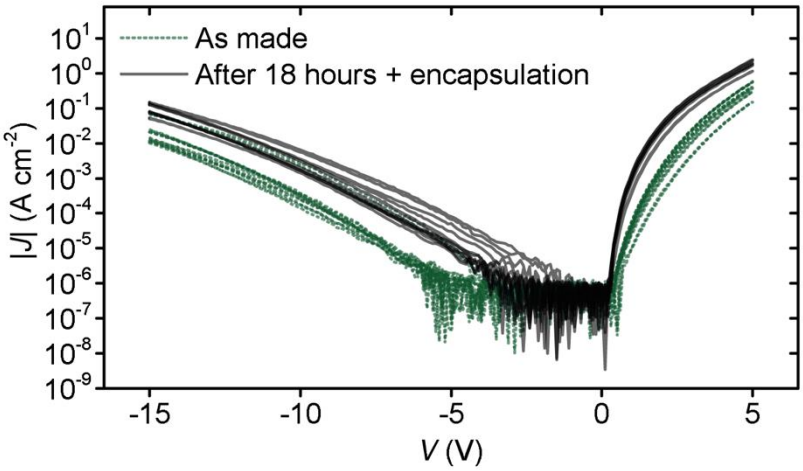

Figure S4. IV characteristics of diodes as fabricated and approximately 18 hours later, showing increase in both on- and off-currents (6/6 devices). Shift in characteristics was seen irrespective of encapsulation. Devices were kept in nitrogen atmosphere between and during tests. Note: measured under short integration conditions.

Supporting Figure S5

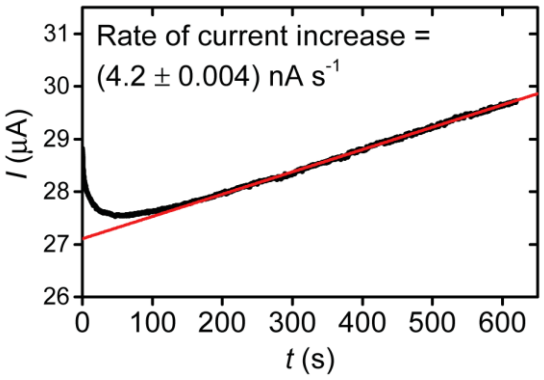

Figure S5. Change in diode on-current (held at V = +5 V) with time, as measured over a ten-minute period. After initially decreasing, most likely due to charging effects, the current value continues to rise uniformly at a rate of 4 nA s^{-1}.

Supporting Figure S6

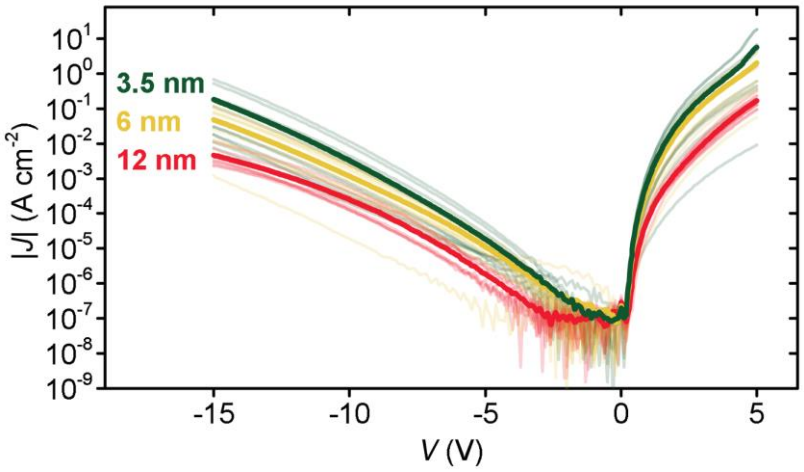

Figure S6. IV characteristics of diodes with varying molybdenum trioxide (MoO_3) thickness: 3.5 nm (10/12 devices), 6 nm (11/12 devices), 12 nm (8/12 devices). Note: measured under short integration conditions.

Supporting Figure S7

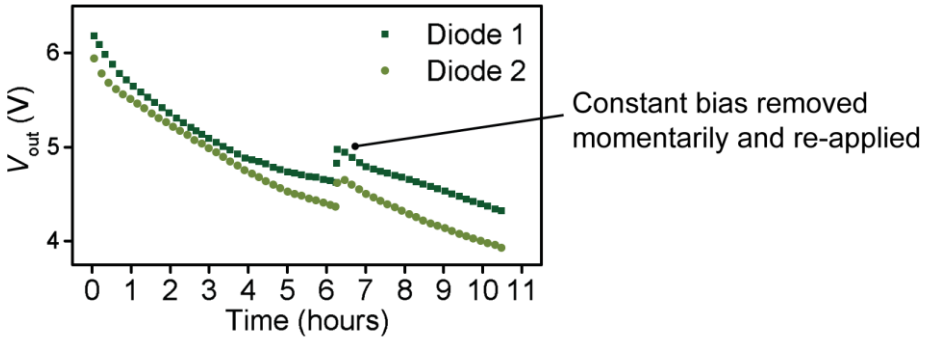

Figure S7. Variation in output voltage for two diodes, both in a half-wave configuration (V_{in} = 20 $V_{p\text{-}p}$, C_L = 1 nF) placed under constant bias for a period of ~10.5 hours. The change at ~6.3 hours was the result of momentarily removing and reapplying the constant bias, suggesting some of the degradation is reversible. Note: due to data loss, these data points were manually extracted from a graphical plot (using WebPlotDigitizer 3.8), hence variation in x-spacing. However, the slight error introduced by this process is considered negligible.

Supporting Figure S8

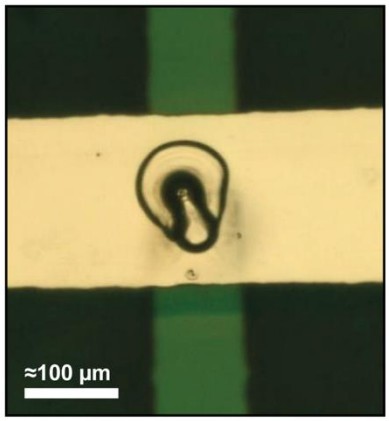

Figure S8. Optical micrograph of diode that has undergone Joule heating and broken down under forward bias. Thermal effects are clearly seen in the center of the image.

Supporting Figure S9

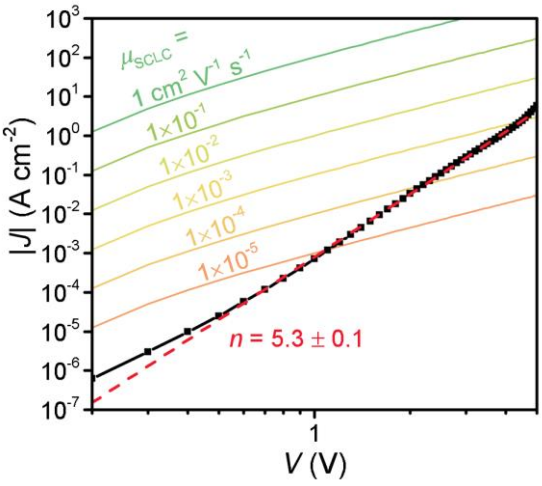

Figure S9. Plot of the IV characteristics of an organic diode, compared to a simulated fit (labelled lines) of theoretical SCLC current density. Dashed line shows a linear fit of IV characteristics for $V > 2$ V.

Simulated fits were calculated using Equation (1) in the main text, repeated here:

$$J = \frac{9}{8}\mu\varepsilon_0\varepsilon_r\frac{(V_{in}-V_T)^2}{L^3} \qquad (1)$$

and using the following device parameters:

$1\times10^{-5} \leq \mu \leq 1$ cm^2 V^{-1} s^{-1}
ε_0 = 8.85×10^{-12} F m^{-1}
ε_r = 1.5 (extracted from capacitance data shown in Figure 2b in the main text)
V_T = 0.1 V
L = 106 nm